Environmental Science and Pollution Research (2018) 25:23315–23327
https://doi.org/10.1007/s11356-018-2439-7

RESEARCH ARTICLE

Conversion of *Eragrostis plana* Nees leaves to activated carbon by microwave-assisted pyrolysis for the removal of organic emerging contaminants from aqueous solutions

Mariene R. Cunha[1] · Eder C. Lima[2] · Nilton F. G. M. Cimirro[1] · Pascal S. Thue[2] · Silvio L. P. Dias[2] · Marcos A. Gelesky[3] · Guilherme L. Dotto[4] · Glaydson S. dos Reis[5] · Flávio A. Pavan[1]

Received: 19 April 2018 / Accepted: 28 May 2018 / Published online: 5 June 2018

Abstract

Eragrostis plana Nees leaves, abundant lignocellulosic biomass, was used as carbon source for preparation of activated carbon, by using microwave-assisted pyrolysis and chemical activation. The novel activated carbon (MWEPN) was characterised by FTIR, CHN elemental analysis, Boehm's titration method, TGA, SEM, N_2 adsorption/desorption curves and pH of the point of zero charge (pH_{pzc}). Afterwards, the adsorbent was successfully employed for adsorption of the two emerging contaminants (caffeine and 2-nitrophenol). The results indicated that MWEPN had a predominantly mesoporous structure with a high surface area of 1250 $m^2\ g^{-1}$. FTIR analysis indicated the presence of carbonyl, hydroxyl and carboxylic groups on the surface of MWEPN. The Boehm analysis showed the existence of the high amount of acid moieties on the surface of activated carbon. Adsorption kinetic indicated that the system followed the Avrami fractional order at the optimal pH of 7. The equilibrium time was attained at 30 min. The Liu isotherm model better described the isothermal data. Based on the Liu isotherm, the maximum sorption capacities (Q_{max}) of caffeine and 2-nitrophenol adsorbed onto activated carbon at 25 °C were 235.5 and 255.8 mg g^{-1}, respectively.

Keywords *Eragrostis plana* Nees leaves · Activated carbon · Microwave-assisted pyrolysis · Emerging contaminant · Caffeine · 2-Nitrophenol

Responsible editor: Philippe Garrigues

Electronic supplementary material The online version of this article (https://doi.org/10.1007/s11356-018-2439-7) contains supplementary material, which is available to authorized users.

✉ Flávio A. Pavan
flavio.pavan@unipampa.edu.br

[1] Federal University of Pampa (UNIPAMPA), Bagé, RS 96412-420, Brazil

[2] Institute of Chemistry, Federal University of Rio Grande do Sul (UFRGS), Av. Bento Gonçalves 9500, P.O. Box 15003, Porto Alegre, RS 91501-970, Brazil

[3] School of Chemistry and Food, Federal University of Rio Grande (FURG), Rio Grande, RS, Brazil

[4] Chemical Engineering Department, Federal University of Santa Maria (UFSM), Santa Maria, RS, Brazil

[5] Metallurgical and Materials Engineering (PPGE3M), School of Engineering, Federal University of Rio Grande do Sul (UFRGS), Av. Bento Gonçalves 9500, Porto Alegre, RS, Brazil

Introduction

Potable water accessibility is prone to decrease in the future due to augmented anthropogenic contaminants from domestic, industrial and agricultural use of water (Unesco 2017). It is estimated that 80% of the world's wastewater is disposed to the environment without any treatment (Unesco 2017). For developing countries, these values can attain up to 95% of the wastewater generated (Unesco 2017). Water pollution is increasing in the natural waters of Asia, Latin America and Africa. Approximately 800,000 deaths worldwide occurred in 2012, due to inappropriate sanitation services and contamination of drinking water (Unesco 2017).

Wastewater from industrial activities may contain toxic organic compounds called as emerging pollutants. These compounds can be defined as any a chemical compound (natural or synthetic) or some microorganism that is not conventionally monitored in the environment but present potential to enter into the environment and cause antagonistic human health

effects or ecological one (Ortigara and Connor, 2017). Emerging pollutants could be divided into some categories, such as personal care products (such sunscreen agents, insect repellents, fragrances, antiseptics and microbeads), hormones, steroids, pharmaceuticals, pesticides and herbicides, flame retardants, surfactants, industrial additives, plasticisers and other chemicals (Norman 2018).

Electrochemical method (Chung et al., 2018), biological method (Wang and Wang, 2017), advanced oxidation process (Barrera-Diaz et al., 2018; Pi et al., 2018) and adsorption (Sophia et al., 2016; Sophia and Lima, 2018) are methods commonly employed for treatment of effluents containing emerging contaminants. These methods can be used for the removal of different pollutants from waters with success. Amongst them, adsorption appears to be more exciting technology for the water treatment (Sophia et al., 2016; Sophia and Lima, 2018).

Activated carbon has been employed extensively as an adsorbent in adsorption processes due to the large surface area, excellent thermal stability, mechanical strength and high volume of pores with a well-developed internal structure of pores. These textural characteristics enhance the adsorption of several adsorbates (Marsh and Rodriguez-Reinoso, 2006; Thue et al., 2017a, b; Umpierres et al., 2018). Activated carbon is usually prepared by physical or chemical activation process (Marsh and Rodriguez-Reinoso, 2006). The physical activation procedure involves pyrolysis of the precursor at inert atmosphere (450–500 °C) and a posterior activation at a higher temperature (850–1100 °C).

In the chemical activation, the carbon source is impregnated with aqueous solutions of inorganic chemicals such as KOH, H_3PO_4, $ZnCl_2$, $FeCl_3$, $CuCl_2$, $NiCl_2$, $CoCl_2$, CaO, H_2SO_4, KOH, NaOH and others (Thue et al., 2017a; Umpierres et al., 2018). In this step, it is advisable to heat the sample to 70–80 °C to react the inorganics with the biomass (Thue et al., 2017b). Subsequently, the carbon material is dried at around 100 °C to expulse the water. Afterwards, the chemically treated carbon material is pyrolysed between 500–850 °C under a nitrogen atmosphere (Thue et al., 2016, 2017b). After the pyrolysis, the obtained material is a composite of carbon and mixture of inorganics, and it is necessary to leach out the inorganic components to achieve the activated carbon with an excellent developed pore structure (Leite et al., 2017b).

Activated carbons can be produced by conventional (Baysal et al., 2018) or microwave heating process (Thue et al., 2017a, b). In traditional pyrolysis, the heating process takes place from outside to inside the sample, and the heat is transferred to the sample by radiation, conduction and convection phenomena. In the microwave method, the heat is directly furnished to the sample considering that microwave is readily transformed into heat inside the particles of the sample by ionic conduction and dipole rotation (Georgina et al., 2016). The microwave radiation is a promising method for the preparation of activated carbons with high adsorption capacities (Cheng et al., 2018; Thue et al., 2016, 2017a, b; Umpierres et al., 2018). Microwave system offers several advantages over the conventional method such as rapid temperature rise, energy savings and increasing yield of the carbon material (Thue et al., 2016, 2017a, b; Umpierres et al., 2018).

The production of activated carbon using different agricultural residues as carbon precursor has drawn the attention of many researchers (Du et al., 2017; Yahya et al., 2015a, b, 2016; Leite et al., 2017b; Namazi et al., 2016; Yahya et al., 2015a, b). In this focus, the present work investigated the applicability of *Eragrostis plana* Nees leaves as carbon precursor for preparation of activated carbon using microwave-assisted pyrolysis.

Eragrostis plana Nees is abundant plant biomass present in diverse regions of Brazil. It is a tropical *Poaceae* exotic originating from Africa and introduced in Brazil in the 1950s (Filho et al., 2017). The *Eragrostis plana* Nees is an invasive species on the farms of Brazil (Barbosa et al., 2013). It presents low nutritional value and high mechanical traction strength. Therefore, it is not appropriate for cattle breeding. Therefore, the *Eragrostis plana* Nees is unsuitable for grazing (Scheffer-Basso et al., 2016). Its presence on the Brazilian farms brings economic losses for farmers (Barbosa et al., 2013). This work aims to add valour to *Eragrostis plana* Nees. For the best of the author's knowledge, there is no study reported in the literature on the preparation of activated carbon from *Eragrostis plana* Nees leaves and its application as an adsorbent for adsorption of the emerging contaminants caffeine and 2-nitrophenol. Caffeine and 2-nitrophenol are present in the Norman list (Norman, 2018). They appear as the number 303 and 539, respectively, in order of priority of emergency of a list of 1036 compounds of emerging concern (Norman, 2018).

Materials and methods

Carbon precursor and chemicals

Eragrostis plana Nees leaves were collected in the region of Bagé Town, Rio Grande do Sul State, Brazil. The biomass was subsequently, washed with tap water to eliminate impurities and then with distilled water and further dried at 60 °C for 72 h. After drying, it was grounded and sieved to obtain desiring particle size. Zinc chloride ($ZnCl_2$) was of analytical grade and was purchased from Neon (São Paulo, Brazil).

The caffeine (see Supplementary Fig. 1) and 2-nitrophenol (see Supplementary Fig. 2) compounds (analytical grade) were procured from Acros Organics (Geel, Belgium) and used as received. Water was purified in a commercial deioniser (Permution, Curitiba, Brazil) and was used to prepare all working solutions.

Preparation of activated carbon adsorbent

The activated carbon was prepared from the microwave pyrolysis process with impregnation ratio of 1:1 (biomass: $ZnCl_2$) according to the literature (Puchana-Rosero et al., 2016). About 100 g zinc chloride plus 100.0 g of dried *Eragrostis plana* Nees leaves and 50 mL water were mixed for forming a smooth paste. The dough resulting was introduced in a quartz reactor, under an N_2 flow rate of 150 mL min^{-1}. This quartz device was placed in a microwave oven and heated up for 320 s (5.3 min) at 1300 W. The pyrolysed material was cooled down using N_2 flow (150 mL min^{-1}). Afterwards, the carbonised sample was refluxed with hydrochloric acid: water 1:1 solution at 80 °C for 2 h (dos Santos et al., 2014) to leach out the inorganic compounds from the carbonaceous matrix (dos Santos et al., 2014). Afterwards, it was extensively washed with deionised water until the washing waters attain the pH values deionised water (dos Santos et al., 2014). Then, this material was dried in an air supply oven overnight at 80 °C. Afterwards, the activated carbon prepared from *Eragrostis plana* Nees leaves, by microwave-assisted pyrolysis, was ground and sieved to particle size lower than 53 μm, and it was called as MWEPN.

MWEPN characterisation

Chemical characterisation of functional groups present on the biomass and the MWEPN activated carbon was obtained by Fourier transform infrared spectroscopy (FTIR) using a spectrophotometer model FTIR-8400S (Shimadzu, Japan). The FTIR spectra were obtained against the background of air spectrum in the range 4000–400 cm^{-1}, using KBr pellets with 0.01 g of samples with a scanning time of 60 s and 4 cm^{-1} resolution (Dotto et al., 2015).

The CHN elemental analysis was carried out using an elemental analyser (Perkin Elmer, Waltham, MA, USA) (Leite et al., 2017a, b).

The total acidity and basicity of functional groups present on the surface of MWEPN were quantified by modified Boehm titration method (Goertzen et al., 2010; Oickle et al., 2010).

Thermogravimetric analyses (TGA) were performed on a TA Instruments model SDT Q600 (New Castle, USA). The temperature was varied from 20 °C up to 700 °C (biomass) or 800 °C (activated carbon) using a heating rate of 10 °C min^{-1}, under N_2 flow rate of 100 mL min^{-1}. For the range of 700 °C (biomass) or 800 °C (activated carbon) to 1000 °C, the purge gas was replaced to synthetic air (100 mL min^{-1}). For the TGA experiments, it was used an acquisition of signal of 12 points per minute, and the weight of the samples was within the range of 10.00–15.00 mg of a sample (Leite et al., 2017a, b).

The scanning electron microscopy technique (SEM) was used to obtain the textural characteristics of raw biomass and activated carbon. An electron microscope (JEOL model JSM-6610LV, Tokio, Japan) operating at 15 kV was used in these measurements (Dotto et al., 2015).

The pore size of MWEPN was calculated by the Barret-Joyner-Halenda (BJH) method obtained from the desorption isotherm at $P/P_0 = 0.95$ (Vaghetti et al., 2003). The surface area (S_{BET}) was determined by the Brunauer, Emmett and Teller (BET) method using N_2 at 77 K after drying sample for 2 h at 150 °C utilising an adsorption analyser (ASAP 2020 Micromeritics Instrument) (Jacques et al., 2007). The micropore volume (V_{mic}) and micropore area (S_{mic}) are obtained using *t*-plot method (dos Reis et al., 2016). The mesopore volume (V_{mes}) was calculated by the subtracting the value of V_{mic} from total volume (V_T). By subtracting S_{mic} from S_{BET}, it is calculated from $S_{external}$ (dos Reis et al., 2016).

The point of zero charge (pH_{pzc}) of MWEPN was obtained according to a previous work (Thue et al., 2016).

Adsorption studies of caffeine and 2-nitrophenol on MWEPN

Batch contact adsorption studies were performed for adsorption of emerging contaminants (caffeine and 2-nitrophenol) from aqueous solutions. A mass (10–200 mg) of MWEPN was added to 20.0 mL solutions of caffeine or 2-nitrophenol at different initial concentrations (100.0–2000.0 mg L^{-1}) and pH values (2.0–10.5). The slurries were then shaken at a controlled temperature orbital shaker for a contact time between 5 to 60 min at 150 rpm. A UV-Vis spectrophotometer (Agilent, Cary 50 Bio, Santa Clara, USA) was used to determine the remaining caffeine and 2-nitrophenol in the solution using 1.0 cm path length cell at a maximum absorption wavelength of caffeine (273 nm) and for 2-nitrophenol (278 nm). The sorption capacity of caffeine and 2-nitrophenol adsorbed on MWEPN at equilibrium (q_e), at any time (q_t) and percentage of removal are expressed in Eqs. (1 and 2) (Leite et al., 2017a, b), respectively:

$$q = \frac{(Co - Cf)}{m} \cdot V \quad (1)$$

$$\%removal = 100 \cdot \frac{(Co - Cf)}{Co} \quad (2)$$

In these equations, q_e is the sorption capacity of the adsorbent at the equilibrium (mg g^{-1}); C_o is the initial adsorbate concentration in contact with the adsorbent (mg L^{-1}); C_f is final adsorbate concentration after the batch adsorption study, respectively (mg L^{-1}); V is the volume of the adsorbate solution (L); and m is the mass of adsorbent (g).

Quality assurance and statistical evaluation of models

See the Supplementary Material (Barbosa-Jr et al., 2000; Lima et al., 1998a, b, 1999, 2015; Schwarz, 1978).

Kinetic models

See the Supplementary Material (Lima et al., 2015).

Equilibrium models

See the Supplementary Material (Lima et al., 2015).

Results and discussion

Characterisation of the activated carbon

The FTIR spectra were obtained to characterise the functional groups present on the surface and the bulk of EPN biomass and MWEPN activated carbon. The FTIR spectra of the EPN biomass and MWEPN activated carbon were recorded as shown in Fig. 1a, b, respectively. The band assignments are shown in Table 1, and they were done according to the literature (Smith et al., 1999). According to these data of the functional group, it could be seen that the EPN is a lignocellulosic material that presents OH groups of aliphatic alcohols, phenol, carboxylic acids or esters and aromatics. The MWEPN presents the following groups, OH of aliphatic alcohols, aromatics and carboxylate. Other groups, such as amine, could be present in the materials; however, due to the high intensity of OH groups at 3100–3500 cm^{-1}, the NH groups could not be observed. Also, phenol groups could be present on the activated carbon, which were not readily detected because of the very intense band at 1038 cm^{-1}. Therefore, the Boehm titration results and C H N analysis should complement these results of FTIR.

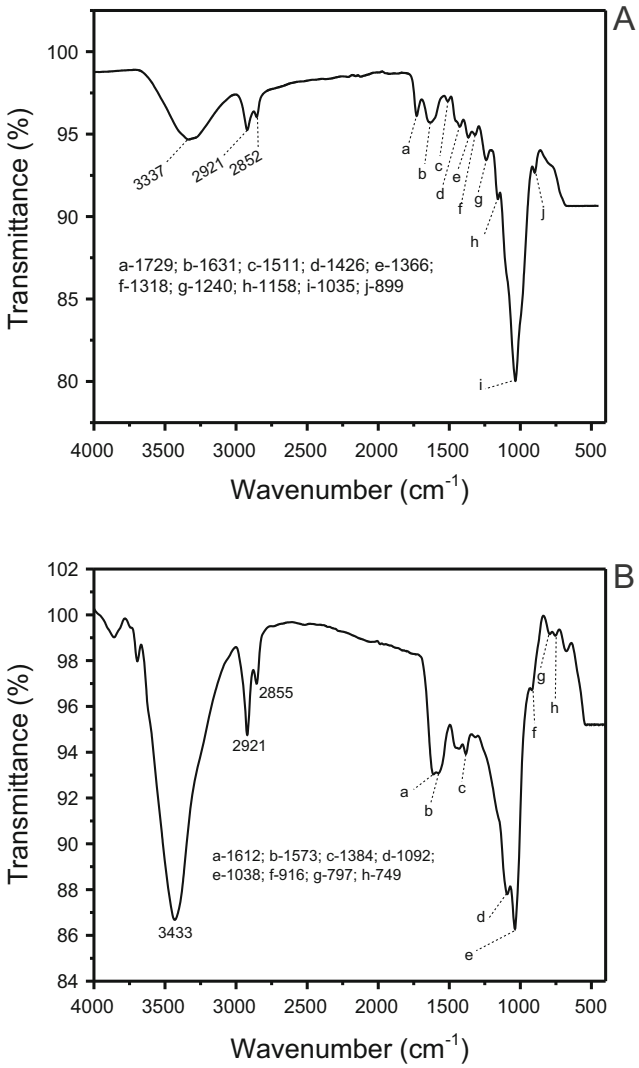

Fig. 1 FTIR spectra of the **a** EPN e and **b** MWEPN

The elemental compositions, carbon, hydrogen, nitrogen and oxygen of biomass precursor (EPN) and derived activated carbon were studied. The results of the elemental analysis show that initially precursor biomass exhibit 48.25% carbon, 6.10% hydrogen, 2.35% nitrogen and 39.64% oxygen. After pyrolysis and leaching out of the inorganics (Umpierres et al., 2018; Thue et al., 2016), the carbon content increase to 66.10%, while the hydrogen, nitrogen and oxygen contents decreased to 3.70, 1.95 and 25.45%, respectively. The rise of carbon content after pyrolysis of biomass is attributed to the dominant aromatic structure of the activated carbon. The

Table 1 FTIR vibrational bands of EPN and MWEPN. Assignments are based on literature (Smith et al., 1999)

Band (cm^{-1})	Assignments
EPN	
3337	O–H stretch
2921	Asymmetric C–H stretching
2855	Symmetric C–H stretching
1729	Asymmetric stretch of carboxylate (C=O)O
1631	Aromatic C=O stretch
1511, 1426	Ring modes of the aromatic ring
1366, 1318	C–H bending
1240	O–C–C stretching of carbonate or C–O of phenol
1158	C–O stretch of secondary alcohols
1035	C–O stretch of primary alcohols
899	CH out of plane bends of aromatic rings
MWEPN	
3433	O–H stretch
2921	Asymmetric C–H stretching
2855	Symmetric C–H stretching
1612	Asymmetric stretch of carboxylate (C=O)O
1573	Ring modes of the aromatic ring
1384	C–H bending
1092	C–O stretch of secondary alcohols
1038	C–O stretch of primary alcohols
916, 797	CH out of plane bends of aromatic rings

losses of hydrogen, nitrogen and oxygen are assigned to the decomposition of the organic fraction such as cellulose, hemicellulose and lignin initially present in biomass precursor during microwave-chemical activation process (Thue et al., 2017b; Tseng et al., 2007). These results were corroborated by the thermal analysis which will be further commented.

The functional groups present on the surface of activated carbon have to influence on its surface properties. The number of chemical groups present on MWEPN surface was determined by the Boehm titration method. The total acidity of MWEPN was 1.040 mmol g^{-1} and the total basicity obtained was only 0.115 mmol g^{-1}. The fractions of carboxylic acid, phenolic and lactone were not performed in this work. Goertzen et al., (2010) and Oickle et al. (2010) reported that it is necessary to expel CO_2 from these diluted solutions using N_2 when carbonate and hydrogen carbonate solutions are used in the Boehm titration (Goertzen et al., 2010; Oickle et al., 2010). Therefore, the total acidity was determined with NaOH solutions and the overall basicity with HCl solutions (Goertzen et al., 2010; Oickle et al., 2010).

The thermal stability of the EPN biomass precursor and MWEPN activated carbon were investigated by thermogravimetric analysis under a nitrogen atmosphere until the weight loss remained constant, up to 700 °C (biomass) or 800 °C (activated carbon) (see Fig. 2). After this temperature, an oxidising atmosphere was imposed with synthetic air from 700 °C (biomass) or 800 °C (activated carbon) up to 1000 °C at a heating rate of 10 °C min^{-1}. This strategy of using a flow of synthetic air for the higher temperature aims to obtain the contents of ash of the samples during the TGA analysis, as early reported in the literature (Thue et al., 2016, 2017b, Leite et al., 2017b). Besides, the pyrolysis of biomass and activated carbon also can be studied, up to 700 °C (biomass) and 800 °C (activated carbon), since for this temperature interval, N_2 is used as purge gas. Figure 2a, b presents the TGA curves of the biomass and MWEPN activated carbon, respectively.

On Fig. 2a, it is possible to see six steps of weight loss, first from 25.1 to 79.1 °C (weight loss of 9.64%) that corresponds to the moisture of samples present on the surface. The second stage from 79.1 to 224.2 °C corresponds to losses of hydration water or water located at the pores of the biomass (Thue et al., 2016, 2017b, Umpierres et al., 2018). The third weight loss (224.2 to 378.9 °C) of biomass was 52.27%, which could be assigned to degradation of hemicelluloses and cellulose (Elizalde-Gonzales and Hernández-Montoya, 2009). The fourth weight loss (12.50%) occurred between 378.9 and 699.9 °C weight loss was attributed to the degradation of lignin (Zhang et al., 2012). The fifth weight loss occurred when the N_2 atmosphere was changed to synthetic air. This weight loss corresponds to the burn-off of practically all the organic matter present in the crucible (weight loss of 15.48%). Moreover, the last weight loss (731.9 to 800.0 °C) is just the elimination of residual carbon from the TGA crucible (weight

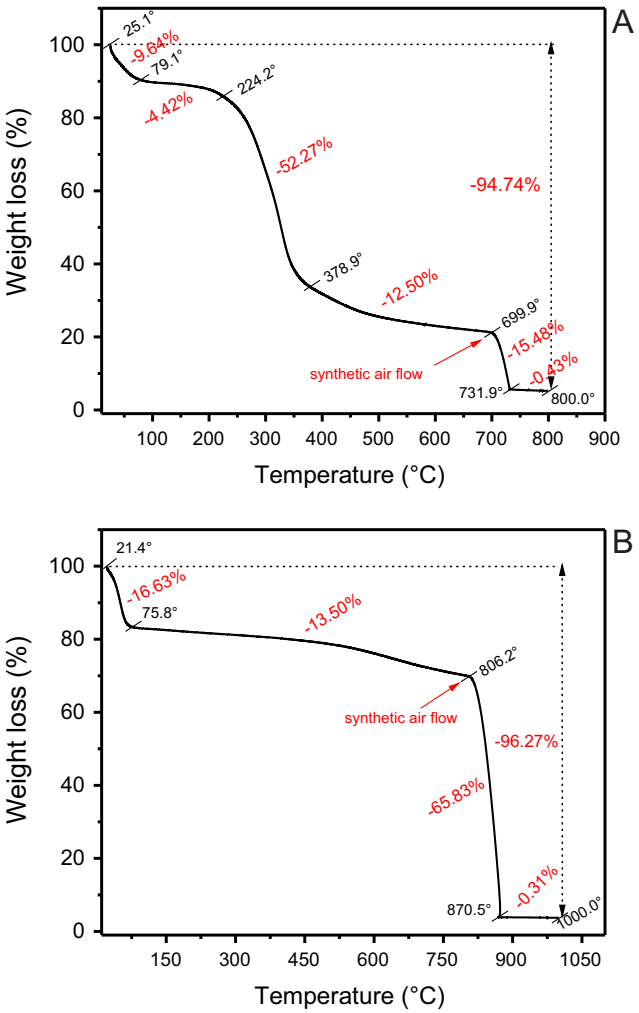

Fig. 2 Thermogravimetric curves of **a** EPN biomass and **b** MWEPN at N_2 atmosphere

loss of only 0.43%). The total weight loss of the biomass was 94.74%, which means that the ash content of biomass is 5.26%. This value was possible to be obtained by using the final step of TGA analysis using synthetic air flow (Thue et al., 2016, 2017b, Umpierres et al., 2018).

Figure 2b shows the thermal behaviour of MWEPN activated carbon. Comparing Fig. 2a of precursor to Fig. 2b, it can be seen that MWEPN activated carbon was more stable at higher temperatures. The thermogram in Fig. 4b indicates four weight loss stages: The first region ranging from 21.4 to 75.8 °C can be assigned to losses of adsorbed water (Elizalde-Gonzales and Hernández-Montoya, 2009; Zhang et al., 2012). The second region ranging from 75.8 to 806.2 °C exhibits 13.50% weight loss which was attributed to the degradation of carbonaceous structure of activated carbon under N_2 flow. When the atmosphere was changed to synthetic air, a sudden weight loss of 65.83% took place (806.2 to 870.5 °C) that is the complete combustion of the carbonaceous matrix by the air. Moreover, the last weight loss (870.5 to 1000.0 °C)

was a minimal weight loss (0.31%) that corresponds to a small release of carbon. The total weight loss of activated carbon was 96.27% that corresponds to an ash content of only 3.73% and that is close to the contents of commercial activated carbons (Bedia et al., 2018).

Pore size distribution is an essential property of the adsorbent. In this study, the average pore diameter of pyrolysed adsorbent was obtained by nitrogen adsorption/desorption at − 196 °C. The BJH plot of pyrolysed adsorbent is shown in Fig. 3a. By analysing the Fig. 3a, it is possible to observe that MWEPN exhibits a narrow pore distribution with pore diameters between 23 and 280 °A (2.3 to 28 nm). Based on the IUPAC classification (Thommes et al., 2015), MWEPN is considered primarily as a mesoporous material (nitrogen isotherm adsorption/desorption hysteresis is type IV, see Fig. 3b). The presence of mesopores on MWEPN structure is essential because these mesoporous acting as a transport channel for adsorbate adsorption that can improve adsorption capacity of the material especially for large size molecules (Yang et al., 2017; Liu et al., 2018).

Table 2 summarises the textural parameters of MWEPN adsorbent. The value of the specific surface area of MWEPN

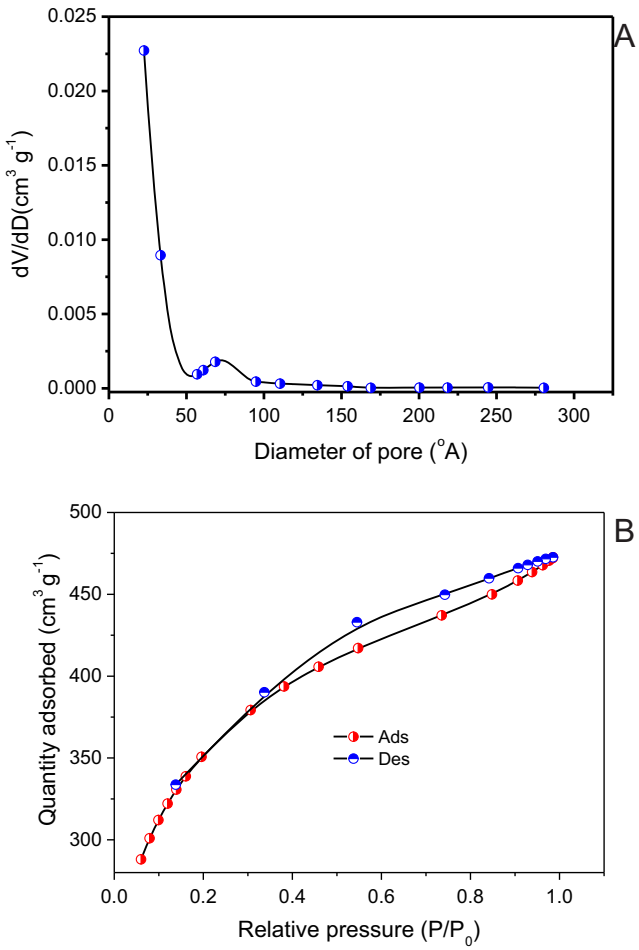

Fig. 3 N_2 adsorption/desorption isotherm **a** BJH and **b** BET

Table 2 The textural properties of MWEPN adsorbent

Characteristics	Values
Specific surface area (S_{BET} (m^2 g^{-1})	1251
Micropore surface area (m^2 g^{-1})	323.8
External surface area (m^2 g^{-1})	927.2
Micropore surface area/S_{BET} (%)	25.88
External surface area/S_{BET} (%)	74.12
Total pore volume (cm^3 g^{-1})	0.7296
Micropore volume (cm^3 g^{-1})	0.1423
Mesopore volume (cm^3 g^{-1})	0.5873
Micropore volume/total pore volume (%)	19.51
Mesopore volume/total pore volume (%)	80.49
Average pore diameter (nm)	2.3–28.0

calculated using BET method was 1251 m^2 g^{-1}. Compared to the others activated carbons previously reported (Gonçalves et al., 2017; Kang et al., 2017; Njoku et al., 2014; Rahman et al., 2017), the surface area of the material prepared in this study appears very competitive. Also, external surface area and the micropore surface area of MWEPN were respectively 927.2 and 323.8 m^2 g^{-1}, which corresponds to 74.12% (external surface area) and 25.88% (micropore area) of the total surface area. Furthermore, MWEPN presents a micropore volume of 0.1423 cm^3 g^{-1} and mesopore volume of 0.5873 cm^3 g^{-1}. Dividing the micropore volume by the total pore volume and the mesopore volume by the total pore volume, the percentage of micropore and mesopore are respectively 19.51 and 80.49%. Based on the results depicted in Table 1, it is possible to make the following statement: 74.12% of the surface area and 80.49% of pore volume are due to mesopores present on the MWEPN activated carbon adsorbent.

Scanning electron microscopy (SEM) was employed to see the textural surface of the carbon source and MWEPN activated carbon. Figure 4a, b presents the images of the surface of biomass precursor (*Eragrostis plana* Nees) and MWEPN activated carbon. These images show that the surface texture of biomass precursor and derived activated carbon are entirely different. SEM image of precursor (Fig. 4a) shows dense and low rugosity material without cavities. While the images of the surface of MWEPN (Fig. 4b) were irregular with large holes that are compatible with a material with high rugosity in its surface (Leite et al., 2017b, Puchana-Rosero et al., 2016). These channels present on the surface of activated carbon allow the passage of the liquid solution through the carbon surface, allowing the mass transfer of the adsorbates from the bulk solution to the surface of the activated carbon (dos Santos et al., 2014; dos Reis et al. 2016).

The point of zero charge (pH_{pzc}) is the pH value that the sum of positive charges and negative charges present on the surface of a solid is zero. The surface of MWEPN can be considered positively charged when pH < pH_{pcz} and

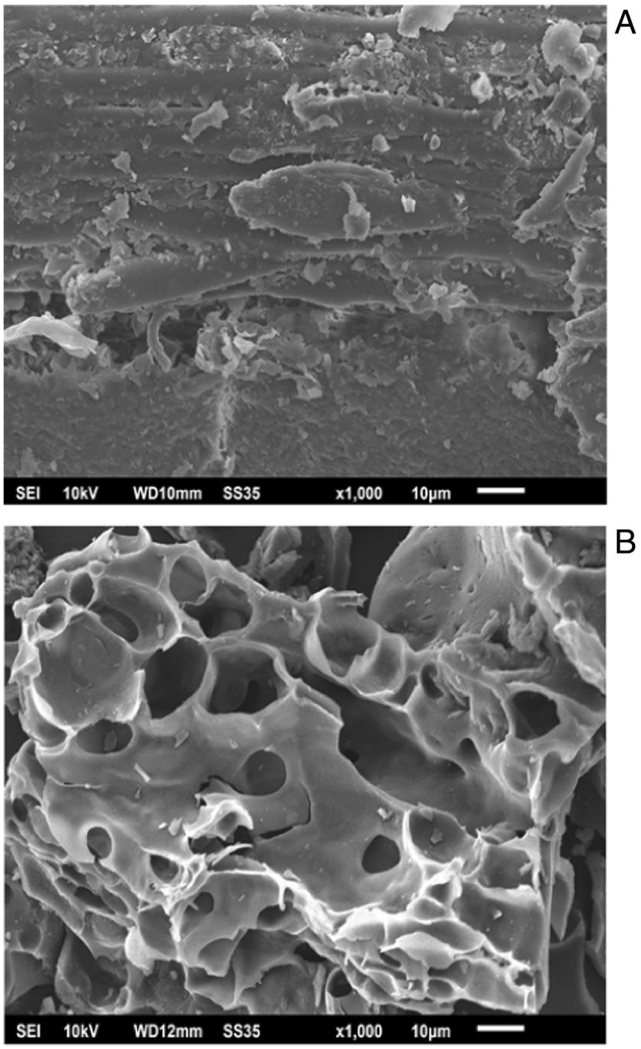

Fig. 4 SEM micrographs **a** EPN biomass and **b** MWEPN materials

negatively charged when pH > pH_{pcz} (Gatabi et al., 2016). Figure 5 illustrates the plot of the difference between the initial and final values versus initial pH values. The pH_{pzc} value of MWEPN was 3.65, indicating the acid character of the activated carbon surface. The results matched with the total acidity amount and basic groups present on MWEPN surface obtained by Boehm titration, as well as with the FTIR data, and C, H, N elemental analysis.

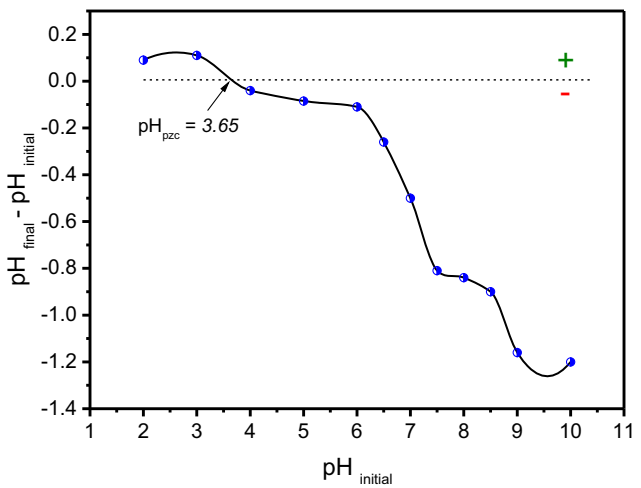

Fig. 5 pH_{pzc} of MWEPN

Optimisation of batch contact adsorption conditions

Batch adsorption studies were performed to remove caffeine and 2-nitrophenol from aqueous solutions. The adsorption studies were carried out at different mass (10-200 mg) of carbon activated into 20.0 mL of caffeine and 2-nitrophenol solutions at initial concentrations ranging from 100.0 to 2000.0 mg/L and pH values from 2.0 to 10.5.

The influence of pH solution of caffeine and 2-nitrophenol adsorption onto MWEPN was investigated and the results obtained are presented in the Fig. 6. According to Fig. 6, it is possible to observe that the efficiency of adsorption of MWEPN for caffeine removal was practically not affected (variations < 0.2%) by the pH of the adsorbate solutions ranging from 2.0 to 10.5. The results indicate that adsorption of caffeine onto MWEPN was not due to electrostatic interaction. For adsorption of 2-nitrophenol onto MWEPN, the effect of the initial pH was slightly higher when compared with caffeine. The maximum variation occurred at pH 2.0 where there was a decrease of 4.2% in the removal percentage to pH 7.0. However, at the pH interval of 5.0 to 8.0, the differences in the percentage of removal were lower than 1.0%. Therefore, it also could be assumed that the electrostatic effect on the adsorption of caffeine and 2-nitrophenol could also be neglected.

The mechanisms of adsorption of emerging contaminants that may take place onto MWEPN activated carbon are van der Waals forces (dispersion interactions, London forces), hydrogen bonds, electron donor-acceptor and π–π interactions (dos Reis et al., 2017; Saucier et al., 2017). The surface of

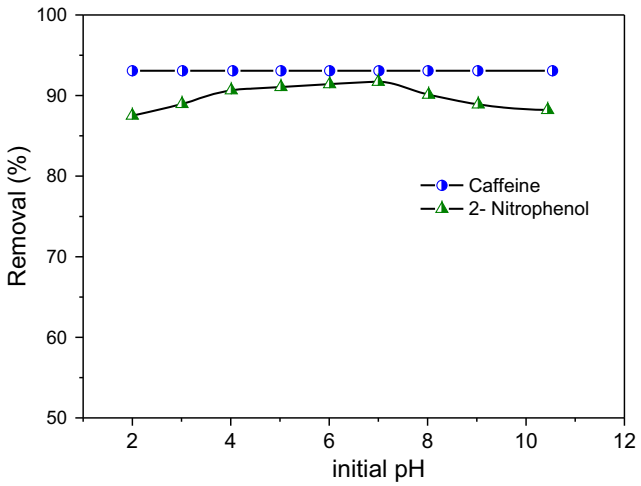

Fig. 6 Effect of pH of the adsorption onto activated carbon *Eragrostis plana* Nees caffeine and 2-nitrophenol. Conditions: $C_0 = 200.0$ mg L^{-1}, $T = 25$ °C, adsorbent mass = 30.0 mg and $t = 60$ min

activated carbons is expected to present significant amounts of polar groups such as –NH, –OH, –O and –COO (shown in the FTIR analysis and Boehm titration) and some polar behaviour (hydrophilic). The organic emerging contaminants adsorption onto activated carbons can occur due to π–π interactions (the π electrons of the aromatic rings of caffeine and 2-nitrophenol with the π electrons of the aromatics present on the MWEPN surface). The donor-acceptor couple is formed with the surface carbonyl groups (electron donors) present on the carbon surface and the aromatic ring of the emerging organic compounds that acts as an acceptor of electrons (dos Reis et al., 2017; Saucier et al., 2017).

The effect of the mass of adsorbent onto emerging organic adsorption was investigated by changing the mass of adsorbent from 10.0 to 200.0 mg. For these studies, others parameters were fixed, such as initial emerging organic contaminant concentration (200.0 mg L^{-1}), initial pH 7, contact time (60.0 min) and stirring speed (150.0 rpm). The adsorbed amount q (mg g^{-1}) and the removed percentage (%Rem) of caffeine and 2-nitrophenol onto MWEPN activated carbons are presented in the Fig. 7. These results show that when the mass of adsorbent increased from 10.0 to 70.0 mg, the percentage of removal risen from 38.5 to 97.8 and 40.9 to 98.9% for caffeine and 2-nitrophenol, respectively. Figure 7 shows that using a mass of 70.0 mg of MWEPN, the percentage of removal and sorption capacities were 97.8% and 55.31 mg g^{-1} for caffeine and 98.9% and 52.86 mg g^{-1} for 2-nitrophenol. Above 70 mg the percentage of removal remained practically unchanged. For this reason, 70 mg was fixed for the other experiments described in this work.

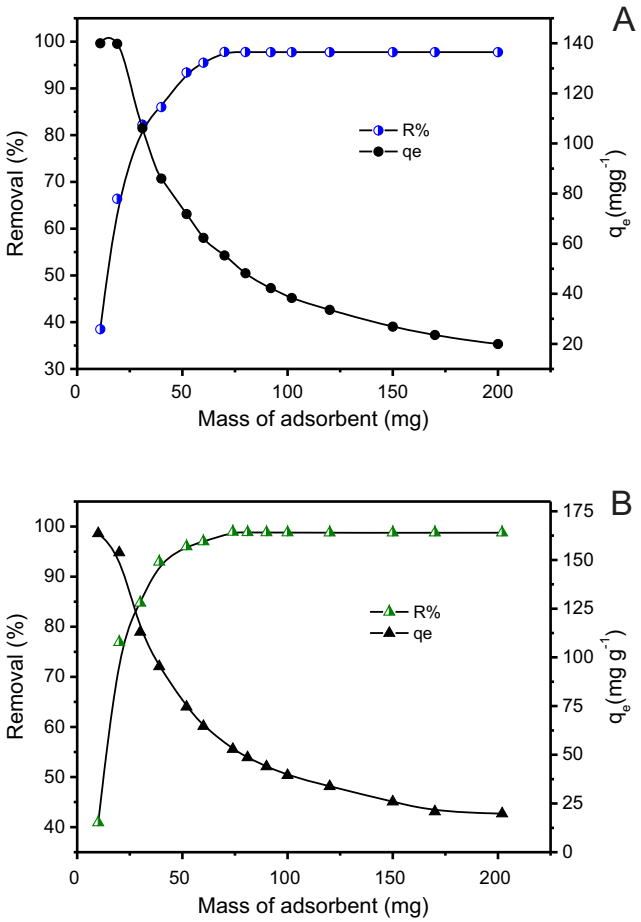

Fig. 7 Effect of mass of the MWEPN on the adsorption. **a** Caffeine. **b** 2-Nitrophenol. Conditions: $C_0 = 200.0$ mg L^{-1}, $T = 25$ °C, $t = 60$ min and pH = 7.0

Increases in the percentage of the emerging contaminant removal with masses of activated carbon up to 70.0 mg could be assigned to rises of surface areas, enhancing the number of active adsorption sites accessible for adsorption of the adsorbate (Alencar et al., 2012). Otherwise, the increase in the adsorbent amount leads to a decrease in the sorption capacity (q). The decrease in q values should be due to two factors. First, the reduction in q values could be assigned to aggregation of particles of the adsorbent, due to high amounts of adsorbent added. Such mass aggregation would lead to a decrease in the total surface area of the activated carbon and an increase in diffusional path length (Alencar et al., 2012). Second, the rise in adsorbent mass at fixed volume and adsorbate concentration and will occur an unsaturation of adsorption sites during the contact of the adsorbent with the adsorbate (Alencar et al., 2012).

Kinetic models

The kinetic data of the adsorption of caffeine and 2-nitrophenol onto activated carbon were explored using pseudo-first-order, pseudo-second-order and fractional Avrami kinetic models (Lima et al., 2015). The kinetic adsorption curves and the parameters of the kinetic model are shown in Fig. 8 and Table 3.

The fitness of the kinetic models was determined by analysing the adjusted determination coefficient (R^2_{Adj}) and standard deviation of residues (SD) (Prola et al., 2013; Thue et al., 2018; Umpierres et al., 2017). Being that, lower SD and higher R^2_{Adj} values reveal the smaller disparity between experimental and theoretical q values (calculated by the models) (Prola et al., 2013; Thue et al., 2018; Umpierres et al., 2017). Therefore, based on the results exhibited in Table 3, the Avrami fractional kinetic adsorption model was the best to explain the kinetic data obtained. The Avrami fractional model presented lower SD (varying from 0.1826 to 0.2554 mg g^{-1} for caffeine and from 0.2414 to 2.582 mg g^{-1} for 2-nitrophenol) and higher R^2_{Adj} values (0.9981–0.9999 for caffeine and 0.9962–0.9994 for 2-nitrophenol, see Table 3). These results indicated that the q_t predicted by the Avrami fractional kinetic model is closest to the values of q_t experimentally measured. Also to complement the comparisons of different kinetic models with a different number of parameters, we used the Bayesian information criterion (BIC) (Schwarz et al., 1978).

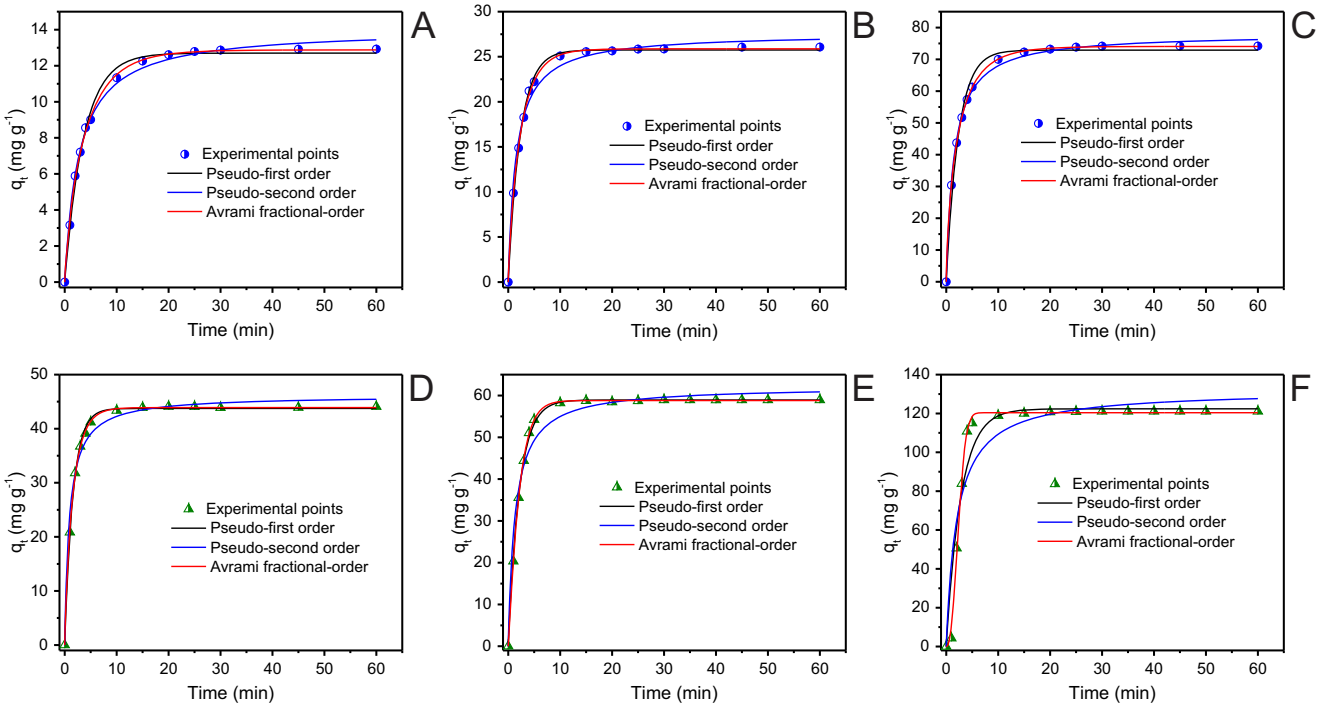

Fig. 8 Kinetic adsorption curves of **a** 50 mg L^{-1} caffeine, **b** 100 mg L^{-1} caffeine, **c** 200 mg L^{-1} caffeine, **d** 50 mg L^{-1} of 2-nitrophenol, **e** 100 mg L^{-1} of 2-nitrophenol and **f** 200 mg L^{-1} of 2-nitrophenol, using MWEPN activated carbon as adsorbent, and the initial pH of adsorbate solution was fixed at pH 7.0, temperature of 25 °C, mass of adsorbent of 70 mg

Table 3 Kinetics parameters for the adsorption of caffeine and 2-nitrophenol on MWEPN. Al values are expressed with four significant digits

	Caffeine (mg L^{-1})			2-Nitrophenol (mg L^{-1})		
Initial concentration	50.0	100.0	200.0	50.0	100.0	200.0
Pseudo-first order						
q_e (mg g^{-1})	12.70	25.75	72.89	43.75	58.94	122.4
k_f (min^{-1})	0.2737	0.4295	0.4288	0.6242	0.4667	0.3522
$t_{1/2}$(min)	2.532	1.614	1.616	1.110	1.485	1.968
R^2_{adj}	0.9948	0.9978	0.9901	0.9986	0.9986	0.9306
SD (mg g^{-1})	0.3044	0.3755	2.221	0.4927	0.6306	11.06
BIC	− 25.40	− 19.94	26.27	− 12.88	− 8.573	83.09
Pseudo-second order						
q_e (mg g^{-1})	14.06	27.60	78.10	46.14	62.21	132.1
k_s (mg g^{-1} min^{-1})	0.02583	0.02405	0.008575	0.02370	0.01220	0.003632
$t_{1/2}$(min)	2.754	1.507	1.493	0.9147	1.317	2.084
R^2_{adj}	0.9944	0.9898	0.9971	0.9861	0.9719	0.8776
SD (mg g^{-1})	0.3186	0.8082	1.196	1.528	2.873	14.69
BIC	− 24.22	− 0.01411	10.17	16.54	39.95	92.17
Avrami fractional						
q_e (mg g^{-1})	12.88	25.87	74.05	43.91	58.79	120.4
k_{AV} (min^{-1})	0.2600	0.4299	0.4259	0.6326	0.4632	0.3664
n_{AV}	0.8426	0.8882	0.7391	0.9063	1.111	2.350
$t_{1/2}$ (min)	2.489	1.540	1.430	1.055	1.552	2.335
$t_{0.95}$ (min)	14.14	8.000	10.36	5.305	5.799	4.353
R^2_{adj}	0.9981	0.9993	0.9999	0.9994	0.9998	0.9962
SD (mg g^{-1})	0.1858	0.2174	0.1826	0.3186	0.2418	2.582
BIC	− 36.91	− 32.83	− 37.37	− 22.89	− 37.66	38.12

As can be seen, all BIC values of the Avrami fractional kinetic model are lower than all values of pseudo-first order and pseudo-second order. Besides that, the difference of pseudo-first-order and Avrami fractional order and pseudo-second-order and Avrami fractional order were always higher than 10, indicating clearly that the model with a lower value of BIC should be the chosen model (Schwarz et al., 1978). Based on this statistical evaluation of R^2_{adj}, SD and BIC values, the best kinetic adsorption model for the obtained data of this work should be Avrami fractional-order kinetic model.

It is a hard task to compare different kinetic constants of different kinetic models, so $t_{1/2}$ and $t_{0.95}$ were used to compare the kinetics of caffeine and 2-nitrophenol onto MWEPN activated carbon (Thue et al., 2016, 2018; Saucier et al., 2017). The $t_{1/2}$ and $t_{0.95}$ are the times (according to the nonlinear fitting curve) to obtain 50 and 95% of the value of q_e, respectively (which represents the saturation of the adsorbent) (Thue et al., 2016, 2018; Saucier et al., 2017).

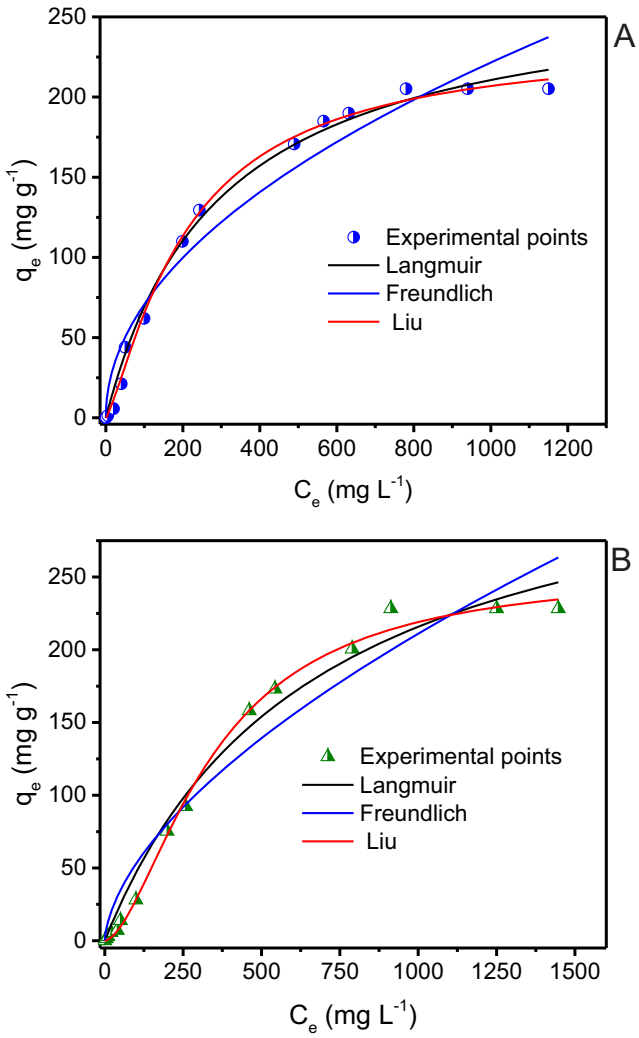

Fig. 9 Equilibrium isotherm curves of **a** caffeine **b** 2-nitrophenol on MWEPN. Conditions: pH = 7.0; T = 25 °C; t = 30 min and mass = 70 mg; time of contact between the adsorbent and adsorbates of 30 min

The work was continued with the following contact time of 30 min for adsorption of caffeine and 2-nitrophenol onto MWEPN activated carbon. This contact times was a little higher than the $t_{0.95}$ of respective pharmaceutical to guarantee enough time for the system to achieve the equilibrium time between adsorbent and adsorbate (Thue et al., 2016, 2018; Saucier et al., 2017).

Equilibrium models

Langmuir, Freundlich and Liu isotherm models were used for analysis of the equilibrium isotherm. The equilibrium data were carried at 25 °C using the following conditions: 30.0 min of contact time between the adsorbent and adsorbate, initial pH of caffeine and 2-nitrophenol solutions was 7.0 and adsorbent mass was 70.0 mg. Figure 9 shows the adsorption isotherms of caffeine and 2-nitrophenol onto MWEPN activated carbon.

Based on the lower *SD* values and R^2_{adj} closer to 1.000, the Liu isotherm model was the best isotherm model tested (Lima et al., 2015; Saucier et al., 2017) (see Table 4). For Liu model, the *SD* values were 5.119 and 5.285 mg g^{-1}, for caffeine and 2-nitrophenol, respectively. For Langmuir isotherm, the *SD* values were 6.946 and 11.98 mg g^{-1}, respectively for caffeine and 2-nitrophenol, respectively. Moreover, for the Freundlich isotherm model, the *SD* values were 17.71 and 21.28 mg g^{-1}

Table 4 Isotherm parameters for caffeine and 2-nitrophenol adsorption onto MWEPN at 25 °C. Al values are expressed with four significant digits

Nonlinear models	Caffeine	2-Nitrophenol
Langmuir		
Q_{max} (mg g^{-1})	272.3	360.5
K_L (L mg^{-1})	0.003414	0.001492
R^2_{adj}	0.9935	0.9843
SD (mg g^{-1})	6.946	11.98
BIC	64.12	80.46
Freundlich		
K_F (mg g^{-1} (mg L^{-1})$^{-1/nF}$)	7.236	3.332
n_F	2.019	1.665
R^2_{adj}	0.9577	0.9504
SD (mg g^{-1})	17.71	21.28
BIC	92.20	97.71
Liu		
Q_{max} (mg g^{-1})	235.5	255.8
K_g (L mg^{-1})	0.004717	0.002895
n_L	1.2750	1.680
R^2_{adj}	0.9965	0.9969
SD (mg g^{-1})	5.119	5.285
BIC	56.48	57.43

for caffeine and 2-nitrophenol, apiece. Also, to complement the comparisons of different isotherm models with a different number of parameters, the BIC (Schwarz et al., 1978) was used. For 2-nitrophenol, the difference of BIC values of Langmuir and Liu and Freundlich and Liu values are higher than 10; therefore, it is clear that Liu is the best isotherm model. However, for caffeine, the difference of BIC values between Langmuir and Liu is 7.64, which could be considered as a reliable tendency of the method with a lower BIC value (Liu) be the best isotherm model (Schwarz et al., 1978).

Considering the Liu isotherm model, the best model for describing the equilibrium data of the two emerging contaminants, the maximum sorption capacity (Q_{max}) obtained were 235.5 and 255.8 mg g^{-1} for caffeine and 2-nitrophenol, respectively.

Conclusions

In this study, the activated carbon was prepared from *Eragrostis plana* Nees (EPN) biomass by chemical activation method using microwave induced pyrolysis. Zinc chloride was used as the chemical activating agent. It was prepared as a paste of biomass: $ZnCl_2$ with a ratio in the mass of 1:1 and followed by drying and further carbonisation in a microwave oven. To eliminate the inorganics utterly present on the carbonised sample, a leaching out procedure with HCl 6.0 mol L^{-1} was carried out. The activated carbon obtained was called as MWEPN. This adsorbent present high surface area (1251 m^2 g^{-1}) and high total pore volume (0.7296 g cm^{-3}). Based on the micropore volume and total pore volume, it could be possible to state that 80.49% of the volume of pores of MWEPN activated carbon is due to mesopores, and only 19.51% are due to micropores. The BJH pore size distribution curve showed that the material presents a region of mesopores. The MWEPN activated carbon was also characterised by CHN elemental analysis, FTIR, SEM, TGA and Boehm titration method and posteriorly used at pH 7 as an alternative adsorbent for the removal of caffeine and 2-nitrophenol from aqueous solution. The FTIR results confirm the presence of functional groups such as −O–H, −C=O, −C–O on the surface of MWEPN. TGA analysis reveals that MWEPN exhibited higher thermal stability event after 750 °C. Boehm titration explains the predominance of acid groups on the surface of MWEPN adsorbent. Contact time of 30 min was chosen as equilibrium time for the caffeine and 2-nitrophenol adsorption. The kinetic and isotherm adsorption were best fitted by the Avrami fractional kinetic model and Liu isotherm model respectively. The maxima adsorption capacity (Q_{max}) were 235.5 and 255.8 mg g^{-1} for caffeine and 2-nitrophenol respectively, at optimised adsorption conditions. The present investigation showed that *Eragrostis plana* Nees can efficiently be used as a carbon precursor for the preparation of activated carbon by chemical activation. The resulting activated carbons may be used efficiently for the removal of caffeine and 2-nitrophenol from aqueous solution.

Acknowledgements The authors are thankful to FAPERGS, CAPES and CNPq for the financial support and sponsorship. We are also thankful to the Centre of Electron Microscopy of the South Zone (CEME-Sul) for the use of the SEM microscope. Also, we are grateful to Chemaxon for furnishing an academic research licence for the Marvin Sketch software, Version 18.9.0, (http://www.chemaxon.com), 2018, used for emerging organic contaminants physical-chemical properties.

References

Alencar WS, Lima EC, Royer B, dos Santos BD, Calvete T, da Silva EA, Alves CN (2012) Application of aqai stalks as biosorbents for the removal of the dye Procion Blue MX-R from aqueous solution. Sep Sci Technol 47: 513–526

Barbosa FG, Pillar VD, Palmer AR, Melo AS (2013) Predicting the current distribution and potential spread of the exotic grass Eragrostis plana Nees in South America and identifying a bioclimatic niche shift during invasion. Austral Ecology 38:260–267

Barbosa-Jr F, Lima EC, Krug FJ (2000) Determination of arsenic in sediment and soil slurries by electrothermal atomic absorption spectrometry using W-Rh permanent modifier. Analyst 125:2079–2083

Barrera-Diaz CE, Frontana-Uribe BA, Rodriguez-Pena M, Gomez-Palma JC, Bilyeu B (2018) Integrated advanced oxidation process, ozonation-electron degradation treatments, for nonylphenol removal in batch and continuous reactor. Catal Today 305:108–116

Baysal M, Bilge K, Yılmaz B, Papila M, Yürüm Y (2018) Preparation of high surface area activated carbon from waste-biomass of sunflower piths: kinetics and equilibrium studies on the dye removal. J Environ Chem Eng 6:1702–1713

Bedia J, Belver C, Ponce S, Rodriguez J, Rodriguez JJ (2018) Adsorption of antipyrine by activated carbons from $FeCl_3$-activation of Tara gum. Chem Eng J 333:58–65

Cheng S, Zhang L, Zhang S, Xia H, Peng J (2018) Preparation of high surface area activated carbon from spent phenolic resin by microwave heating and KOH activation. High Temp Mat Proc 37:59–68

Chung CM, Hong SW, Cho K, Hoffmann MR (2018) Degradation of organic compounds in wastewater matrix by electrochemically generated reactive chlorine species: kinetics and selectivity. Catal Today, in press, doi/https://doi.org/10.1016/j.cattod.2017.10.027

dos Reis GS, Adebayo MA, Sampaio CH, Lima EC, Thue PS, de Brum IAS, Dias SLP, Pavan FA (2017) Removal of phenolic compounds from aqueous solutions using sludge-based activated carbons prepared by conventional heating and microwave-assisted pyrolysis. Water Air Soil Pollut 228(article 33):1–17

dos Santos DC, Adebayo MA, Pereira SFP, Prola LDT, Cataluña R, Lima EC, Saucier C, Gally CR, Machado FM (2014) New carbon composite adsorbents for the removal of textile dyes from aqueous solutions: kinetic, equilibrium, and thermodynamic studies. Korean J Chem Eng 31:1470–1479

Dotto GL, Santos JMN, Rodrigues IL, Rosa R, Pavan FA, Lima EC (2015) Adsorption of methylene blue by ultrasonic surface modified chitin. J Colloid Interf Sci 446:133–140

Du C, Xue Y, Wu Z, Wu Z (2017) Microwave-assisted one-step preparation of macadamia nut shell-based activated carbon for efficient adsorption of Reactive Blue. New J Chem 41:15373–15383

Elizalde-Gonzales MP, Hernández-Montoya V (2009) Guava seeds as an adsorbent and as a precursor of carbon for the adsorption of acid dyes. Bioresour Tecnol 100:2111–2117

Filho ACD, Mazzocato AC, Dotto GL, Thue PS, Pavan FA (2017) *Eragrostis plana Nees* as a novel eco-friendly adsorbent for removal

of crystal violet from aqueous solutions. Environ Sci Pollut Res 24: 19909–19919

Gatabi MP, Moghaddam HM, Ghorbani M (2016) Point of zero charge of maghemite decorated multiwalled carbon nanotubes fabricated by chemical precipitation method. J Mol Liq 216:117–125

Georgina J, Dotto GL, Mazutti MA, Foletto EL (2016) Preparation of activated carbon from peanut shell by conventional pyrolysis and microwave irradiation-pyrolysis to remove organic dyes from aqueous solutions. J Environ Chem Eng 4:266–275

Goertzen SL, Theriault KD, Oickle AM, Tarasuk AC, Andreas HA (2010) Standardization of the Boehm titration. Part I. CO_2 expulsion and endpoint determination. Carbon 48:1252–1261

Gonçalves GC, Nakamura PK, Furtado DF, Veit MT (2017) Utilization of brewery residues to produces granular activated carbon and bio-oil. J Clean Prod 168:908–916

Jacques RA, Bernardi R, Caovila M, Lima EC, Pavan FA, Vaghetti JCP, Airoldi C (2007) Removal of Cu(II), Fe(III) and Cr(III) from aqueous solution by aniline grafted silica gel. Sep Sci Technol 42:591–609

Kang XN, Zhu H, Wang CY, Sun K, Yin J (2017) Biomass-derived hierarchically porous and heteroatom-doped carbons for supercapacitors. J Colloid Interface Sci 509:369–383

Leite AJB, Lima EC, dos Reis GS, Thue PS, Saucier C, Rodembusch FS, Dias SLP, Umpierres CS, Dotto GL (2017a) Hybrid adsorbents of tannin and APTES (3-amino-propyl-triethoxy-silane) and their application for the highly efficient removal of acid red 1 dye from aqueous solutions. J Environ Chem Eng 5:4307–4318

Leite AJB, Sophia AC, Thue PS, dos Reis GS, Dias SLP, Lima EC, Vaghetti JCP, Pavan FA, de Alencar WS (2017b) Activated carbon from avocado seeds for the removal of phenolic compounds from aqueous solutions. Desalin Water Treat 71: 168–181

Lima EC, Fenga PG, Romero JR, de Giovani WF (1998a) Electrochemical behaviour of $[Ru(4,4'\text{-}Me_2bpy)_2(PPh_3)(H_2O)](ClO_4)_2$ in homogeneous solution and incorporated into carbon paste electrodes. Application to oxidation of benzylic compounds. Polyhedron 17: 313–318

Lima EC, Krug FJ, Nóbrega JA, Nogueira ARA (1998b) Determination of ytterbium in animal faeces by tungsten coil electrothermal atomic absorption spectrometry. Talanta 47:613–623

Lima EC, Barbosa-Jr F, Krug FJ, Guaita U (1999) Tungsten-rhodium permanent chemical modifier for lead determination in digests of biological materials and sediments by electrothermal atomic absorption spectrometry. J Anal At Spectrom 14:1601–1605

Lima EC, Adebayo MA, Machado FM (2015) Chapter 3: kinetic and equilibrium models of adsorption, in Carbon nanomaterials as adsorbents for environmental and biological applications, Bergmann CP, Machado FM, Eds. Springer International Publishing, pp. 33–69

Liu F, Dai YX, Zhang S, Li JM, Zhao CC, Wang YQ, Liu CS, Sun J (2018) Modification and application of mesoporous carbon adsorbent for removal of endocrine disruptor bisphenol A in aqueous solutions. J Mater Sci 53:2337–2350

Marsh H, Rodriguez-Reinoso F (2006) Activated carbon, chapter 2—porosity in carbons: modelling, pp 13–86 Elsevier

Namazi AB, Allen DG, Jia CQ (2016) Benefits of microwave heating method in production of activated carbon. Can J Chem Eng 94: 1262–1268

Njoku VO, Islam MA, Asif M, Hammed BH (2014) Preparation of mesoporous activated carbon from coconut frond for the adsorption of carbofuran insecticide. J Anal Appl Pyrolysis 110:172–180

Norman (2018) Network of reference laboratories, research centres and related organisations for monitoring of emerging environmental substances. www.norman-network.net

Oickle AM, Goertzen SL, Hopper KR, Abdalla YO, Andreas HA (2010) Standardization of the Boehm titration: part II. Method of agitation, effect of filtering and dilute titrant. Carbon 48:3313–3322

Ortigara ARC, Connor R (2017) Chapter 4—technical aspects of wastewater in the United Nations Wold Water Development Report - UNESCO

Pi Y, Li X, Xia Q, Wu J, Li Z (2018) Adsorptive and photocatalytic removal of persistent organic pollutants (POPs) in water by metal-organic frameworks (MOFs). Chem Eng J 337:351–371

Prola LDT, Machado FM, Bergmann CP, de Souza FE, Gally CR, Lima EC, Adebayo MA, Dias SLP, Calvete T (2013) Adsorption of Direct Blue 53 dye from aqueous solutions by multi-walled carbon nanotubes and activated carbon. J Environ Manag 130:166–175

Puchana-Rosero MJ, Adebayo MA, Lima EC, Machado FM, Thue PS, Vaghetti JCP, Umpierres CS, Gutterres M (2016) Microwave-assisted activated carbon obtained from the sludge of tannery-treatment effluent plant for removal of leather dyes. Colloid Surf A 504:105–115

Rahman A, Kishimoto N, Urabe T, Ikeda K (2017) Methylene blue removal by carbonized textile sludge-based adsorbent. Water Sci Technol 76:3126–3134

dos Reis GS, Mahbub MKB, Wilhelm M, Lima EC, Sampaio CH, Saucier C, Dias SLP (2016) Activated carbon from sewage sludge for removal of sodium diclofenac and nimesulide from aqueous solutions. Korean J Chem Eng 33: 3149–3161

Saucier C, Karthickeyan P, Ranjithkumar V, Lima EC, dos Reis GS, de Brum IAS (2017) Efficient removal of amoxicillin and paracetamol from aqueous solutions using magnetic activated carbon. Environ Sci Pollut Res 24: 5918–5932

Scheffer-Basso SM, Cecchin K, Favaretto A (2016) Dynamic of dominance, growth and bromatology of Eragrostis plana Nees in secondary vegetation area. Rev Cienc Agron 47:582–588

Schwarz GE (1978) Estimating the dimension of a model. Ann Stat 6: 461–464

Smith B (1999) Infrared spectral interpretation—a systematic approach. CRC Press, Boca Raton

Sophia AC, Lima EC (2018) Removal of emerging contaminants from the environment by adsorption. Ecotox Environ Safe 150:1–17

Sophia AC, Lima EC, Allaudeen N, Rajan S (2016) Application of graphene-based materials for adsorption of pharmaceutical traces from water and wastewater—a review. Desalin Water Treat 57: 27573–27586

Thommes M, Kaneko K, Neimark AV, Olivier JP, Rodriguez-Reinoso F, Rouquerol J, Sing KSW (2015) Physisorption of gases, with special reference to the evaluation of surface area and pore size distribution (IUPAC Technical Report). Pure Appl Chem 87:1051–1069

Thue PS, Adebayo MA, Lima EC, Sieliechi JM, Machado FM, Dotto GL, Vaghetti JCP, Dias SLP (2016) Preparation, characterization and application of microwave-assisted activated carbons from wood chips for removal of phenol from aqueous solution. J Mol Liq 223:1067–1080

Thue PS, dos Reis GS, Lima EC, Sieliechi JM, Dotto GL, Wamba AGN, Dias SLP, Pavan FA (2017a) Activated carbons from Sapelli wood sawdust by microwave-heating process for o-cresol adsorption. Res Chem Intermediat 43:1063–1087

Thue PS, Lima EC, Sieliechi JM, Saucier C, Dias SLP, Vaghetti JCP, Rodembusch FS, Pavan FA (2017b) Effects of first-row transition metals and impregnation ratios on the physicochemical properties of microwave-assisted activated carbons from wood biomass. J Colloid Interface Sci 486:163–175

Thue PS, Sophia AC, Lima EC, Wamba AGN, de Alencar WS, dos Reis GS, Rodembusch FS, Dias SLP (2018) Synthesis and characterization of a novel organic-inorganic hybrid clay adsorbent for the removal of acid red 1 and acid green 25 from aqueous solutions. J Clean Prod 171:30–44

Tseng RL (2007) Physical and chemical properties and adsorption type of activated carbon prepared from plum kernels by NaOH activation. J Hazard Mater 147:1020–1027

Umpierres CS, Prola LDT, Adebayo MA, Lima EC, dos Reis GS, Kunzler DDF, Dotto GL, Arenas LT, Benvenutti EV (2017) Mesoporous Nb_2O_5/SiO_2 material obtained by sol-gel method and applied as adsorbent of Crystal Violet dye. Environ Technol 38:566–578

Umpierres CS, Thue PS, Lima EC, dos Reis GS, de Brum IAS, de Alencar WS, Dias SLP, Dotto GL (2018) Microwave activated carbons from Tucumã (*Astrocaryum aculeatum*) seed for efficient removal of 2-nitrophenol from aqueous solutions. Environ Technol 39: 1173–1187

UNESCO WWDR (2017) The United Nations World Water Development Report. Wastewater: the untapped resource

Vaghetti JCP, Zat M, Bentes KRS, Ferreira LS, Benvenutti EV, Lima EC (2003) 4-Phenylenediaminepropylsilica xerogel as a sorbent for copper determination in waters by slurry-sampling ETAAS. J Anal At Spectrom 18:376–380

Wang S, Wang J (2017) Carbamazepine degradation by gamma irradiation coupled to biological treatment. J Hazard Mater 321:639–646

Yahya MA, Al-Qodh Z, Nghah CWZ (2015a) Agricultural bio-waste materials as potential sustainable precursors used for activated carbon production: a review. Renew Sust Energ Rev 46: 218–235

Yahya MA, Al-Qodah Z, Ngah C, Hashim MA (2015b) Preparation and characterization of activated carbon from desiccated coconut residue by potassium hydroxide. Asian J Chem 27:2331–2336

Yahya MA, Zanariah CW, Ngah CW, Hashim MA, Al-Qodah Z (2016) Preparation of activated carbon from desiccated coconut residue by chemical activation with NaOH. J Mater Sci Res 5:24–31

Yang F, Sun L, Xie W, Jiang Q, Gao Y, Zhang W, Zhang Y (2017) Nitrogen-functionalization biochars derived from wheat straws via molten salt synthesis: an efficient adsorbent for atrazine removal. Sci Total Environ 607:1391–1399

Zhang M, Resende FLP, Moutsoglou A, Raynie DE (2012) Pyrolysis of lignin extracted from prairie cordgrass, aspen, and kraft lignin by Py-GC/MS and TGA/FTIR. J Anal Appl Pyroly 98:65–71

Supplementary Material.

Eragrostis plana Nees leaves as a carbon source for preparation of activated carbon by microwave assisted pyrolysis. Removal of organic emerging contaminants from aqueous solution

Mariene R. Cunha, Eder C. Lima, Nilton F.G.M. Cimirro, Pascal S. Thue, Silvio L. P. Dias, Marcos A. Gelesky, Guilherme L. Dotto, Glaydson S. dos Reis, Flávio A. Pavan*.

2.5. Quality assurance and statistical evaluation of models

All the experiments were carried out in triplicate to ensure reproducibility, reliability and accuracy of the experimental data. The relative standard deviations of all measurements were below 5% (Barbosa-Jr. et al, 2000). Blanks were run in parallel and corrected when necessary (Lima et al., 1998b).

The solutions of caffeine and 2-nitrophenol were stored in glass bottles, which were cleaned by immersing in 1.4 mol L^{-1} HNO_3 for 24 h (Lima et al., 1999), rinsing with deionised water, drying and storing them in a suitable cabinet.

Standard adsorbate solutions (10.0-60.0 mg L^{-1}) were used for calibration in parallel with a blank. All the measurements were performed in triplicate, and the precisions of the standards were better than 4% (n=3) (Lima et al., 1998a).

The kinetic and equilibrium data fitness was done using nonlinear methods, which were evaluated using Simplex method, and the Levenberg–Marquardt algorithm using the fitting facilities of the Microcal Origin 2015 software (Lima et al., 2015). The adequacy of the kinetic and equilibrium models was evaluated using the residual sum of squares (*RSS*), the determination coefficient (R^2), the adjusted determination coefficient (R^2_{adj}), the standard

deviation of residues (*SD*), and also the Bayesian Information Criterion (*BIC*). Equations 3 to 7 are the mathematical expressions for respective *RSS*, R^2, R^2_{adj}, *SD, and BIC*.

$$RSS = \sum_i^n \left(q_{i,\,exp} - q_{i,\,model}\right)^2 \tag{3}$$

$$R^2 = \left(\frac{\sum_i^n \left(q_{i,exp} - \bar{q}_{exp}\right)^2 - \sum_i^n \left(q_{i,\,exp} - q_{i,\,model}\right)^2}{\sum_i^n \left(q_{i,exp} - \bar{q}_{exp}\right)^2} \right) \tag{4}$$

$$R^2_{adj} = 1 - \left(1 - R^2\right) . \left(\frac{n-1}{n-p-1} \right) \tag{5}$$

$$SD = \sqrt{\left(\frac{1}{n-p} \right) . \sum_i^n \left(q_{i,\,exp} - q_{i,\,model}\right)^2} \tag{6}$$

$$BIC = \mathrm{nLn}\left(\frac{RSS}{n} \right) + pLn(n) \tag{7}$$

In the above equations, $q_{i,\,model}$ is individual theoretical q value predicted by the model; $q_{i,\,exp}$ is particular experimental q value; $\bar{q}_{exp}$ is the average of all experimental q values measured; n is the number of experiments; p is the number of parameters in the fitting model.

For comparison of different models of kinetics and equilibrium presented in this work, it will be displayed the values of R^2_{adj}, SD, and BIC. The best-fitted model would introduce R^2_{adj} closer to 1.000, lower values of SD and lower values of BIC. The kinetic and equilibrium model could not merely be chosen based on the values of R^2 (Lima et al., 2015) when these models present a different number of parameters. Therefore, it is necessary to check if the improvements of the R^2 values are due to the increase of the number of the parameters (Lima et al., 2015) or if physically the model with more parameters explains better the process that is taking place (Lima et al., 2015). However, the difference of BIC values between models could be conclusive if the difference of BIC values ≤ 2.0, it is preferable to use the model with the lower number of parameters (Schwarz, 1978). When the difference of BIC values are within 2-6, there is a positive perspective that the model with lower BIC is the most suitable (Schwarz, 1978). For

variations of BIC values from 6-10, there is a strong possibility of the model with lower BIC value be the best model to be fitted [33]. However, if the difference of BIC values ≥ 10.0, the model with the lower value of *BIC* is certainly the best model (Schwarz, 1978).

2.6. Kinetic models

Kinetic data were analysed using pseudo-first order, pseudo second-order and the Avrami-fractional kinetic models (Lima et al., 2015). The mathematical relations of pseudo-first order, pseudo second-order and Avrami-fractional kinetic models are shown in Equations 8, 9 and 10, respectively.

$$q_t = q_e \cdot \left[1\text{-}exp(\text{-}k_F \cdot t)\right] \tag{8}$$

$$q_t = q_e - \frac{q_e}{\left[k_s(q_e)\cdot t + 1\right]} \tag{9}$$

$$q_t = q_e \cdot \left\{1 - exp\left[-\left(k_{AV}.t\right)\right]^{nAV}\right\} \tag{10}$$

In these equations, t is the contact time (min). q_t, q_e are the amount of adsorbate adsorbed at time t and at the equilibrium, respectively (mg g^{-1}). k_F is the pseudo-first-order rate constant (min^{-1}). k_s is the pseudo-second-order rate constant (g mg^{-1} min^{-1}). k_{AV} is the Avrami fractional-order constant rate (min^{-1}). n_{AV} is a fractional kinetic order (Avrami).

2.7. Equilibrium models

Langmuir, Freundlich and Liu models were employed for analysis of equilibrium data. Equations 11, 12 and 13 show the corresponding Langmuir, Freundlich, and Liu models (Lima et al., 2015).

$$q_e = \frac{Q_{\max} \cdot K_L \cdot C_e}{1 + K_L \cdot C_e} \quad (11)$$

$$q_e = K_F \cdot C_e^{1/n_F} \quad (12)$$

$$q_e = \frac{Q_{\max} \cdot (K_g \cdot C_e)^{n_L}}{1 + (K_g \cdot C_e)^{n_L}} \quad (13)$$

In these equilibrium equations, q_e is the adsorbate amount adsorbed at equilibrium (mg g^{-1}). C_e is the adsorbate concentration at equilibrium (mg L^{-1}). Q_{max} is the maximum sorption capacity of the adsorbent (mg g^{-1}). K_L is the Langmuir equilibrium constant (L mg^{-1}). K_F is the Freundlich equilibrium constant [$mg.g^{-1}.(mg.L^{-1})^{-1/nF}$]. K_g is the Liu equilibrium constant (L mg^{-1}). n_F and n_L are the exponents of Freundlich and Liu model, respectively, (n_F and n_L are dimensionless).

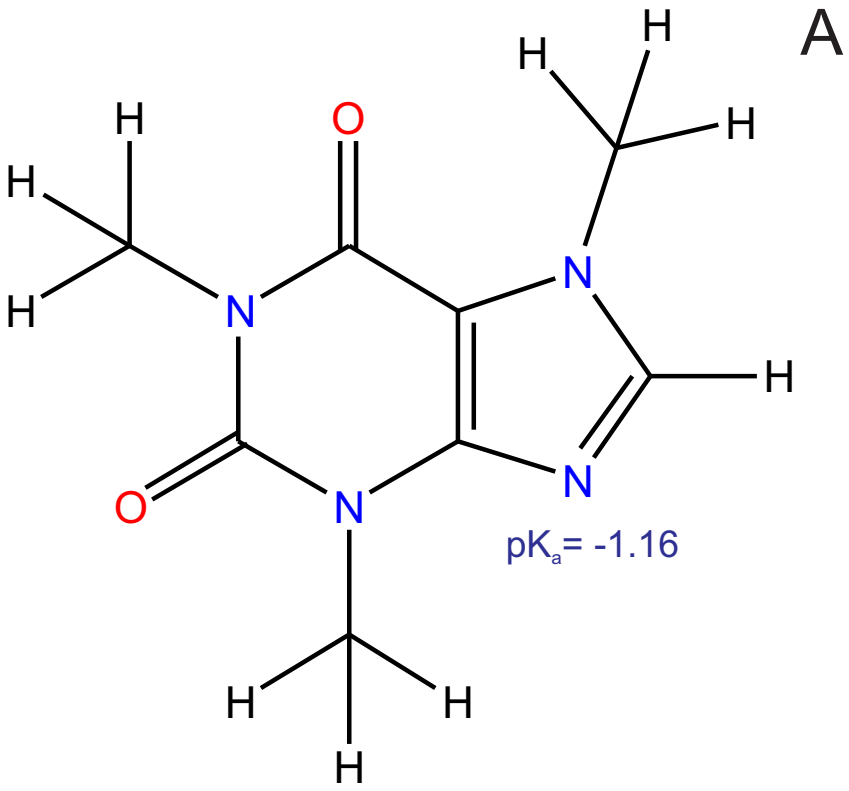

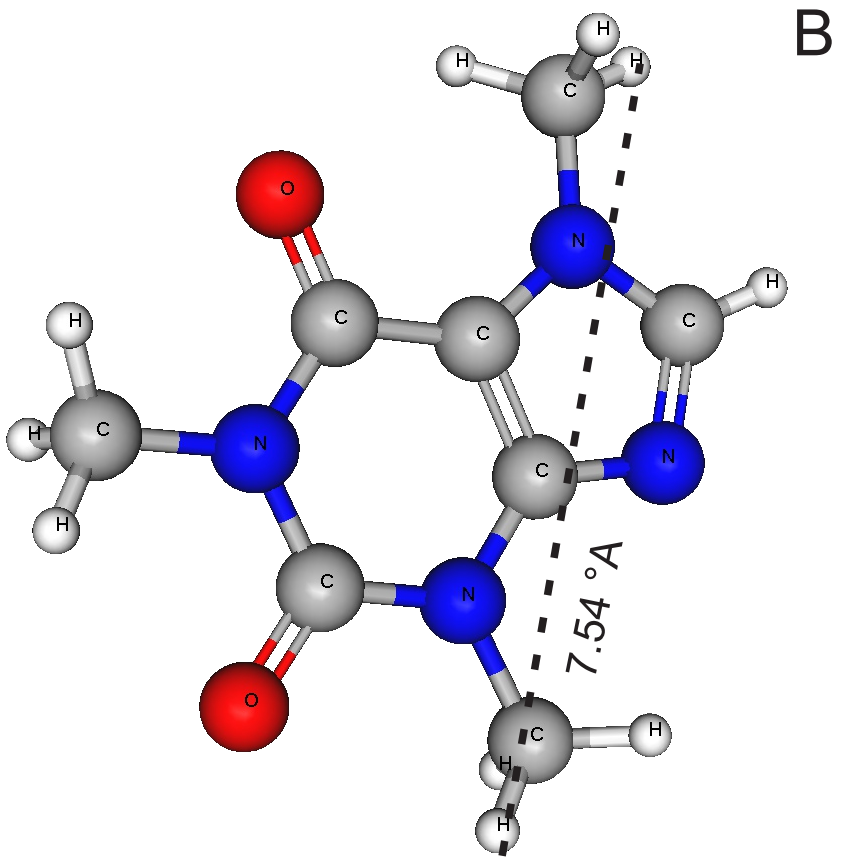

Supplementary Fig 1. A) Structural formula of caffeine (194.194 g mol^{-1}, CAS 58-08-2); B) Optimized three-dimensional structural formula of caffeine. The dimensions of the chemical molecule was calculated using MarvinSketch version 18.9.0. Van der Waals volume 164.20 A^3; Van der Waals surface area 269.07 A^2 (pH 7.0); Polar surface area 58.44 A^2 (pH 7.0); Dipole Moment 5.21 Debye; Log P -0.07; Solubility 21.6 g L^{-1}.

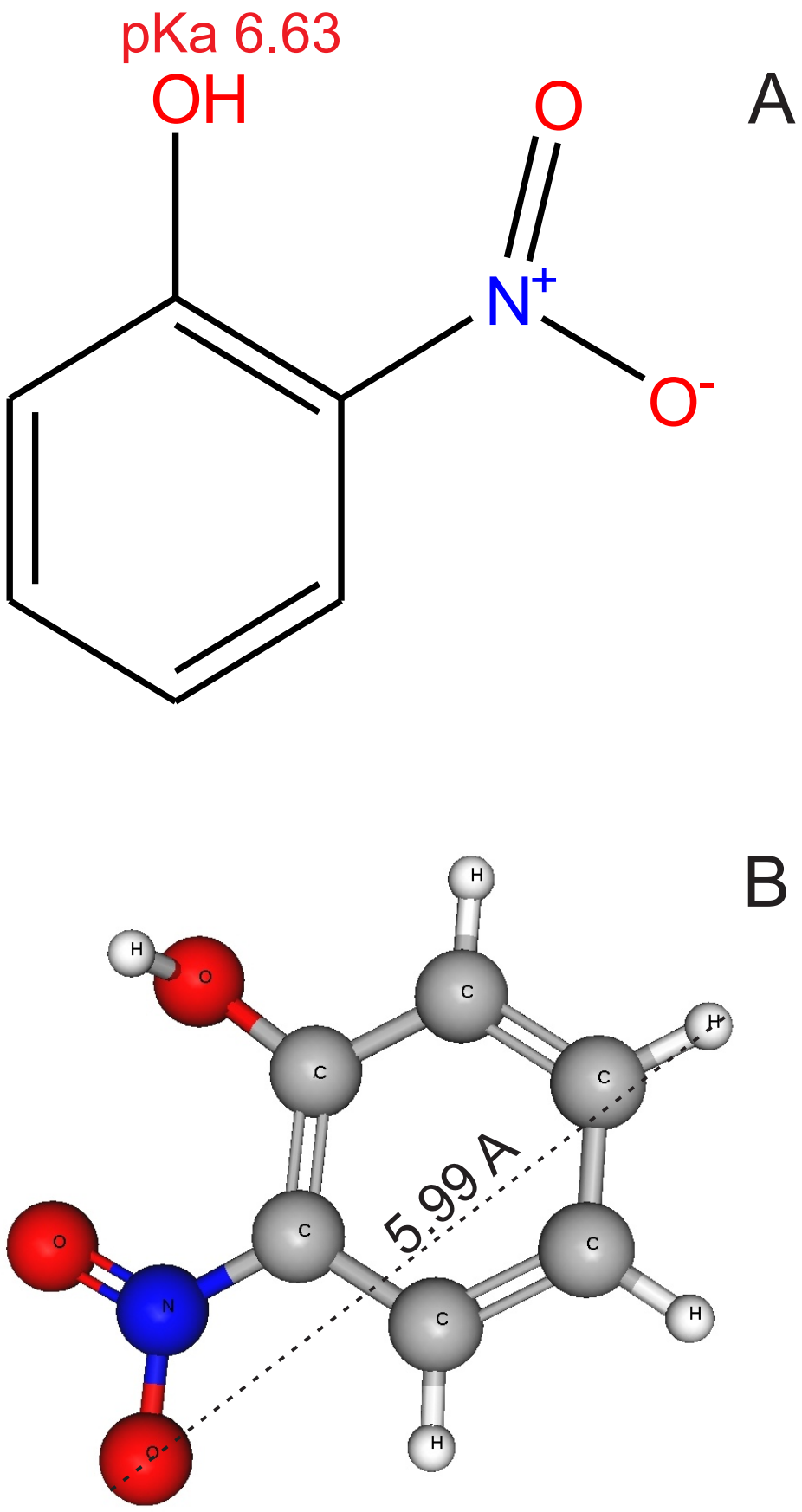

Supplementary Fig 2. A) Structural formula of 2-nitrophenol (139.110 g mol^{-1}, CAS 88-75-2); B) Optimized three-dimensional structural formula of 2 nitrophenol. The dimensions of the chemical molecule was calculated using MarvinSketch version 18.9.0. Van der Waals volume = 113.53 A^3; Van der Waals surface area 184.87 A^2 (pH 7.0); Polar surface area 63.37 A^2 (pH 7.0); Dipole Moment 10.48 Debye; Log P 1.79; Solubility 2.5 g L^{-1}.